RSC Sustainability

ROYAL SOCIETY OF CHEMISTRY

COMMUNICATION

View Article Online
View Journal | View Issue

Cite this: *RSC Sustainability*, 2024, **2**, 2839

Received 2nd August 2024
Accepted 29th August 2024

DOI: 10.1039/d4su00434e

rsc.li/rscsus

Engineered hole-free, spacer-free dye-sensitized light harvesters for indoor photovoltaic and self-powered applications†

Andrew Simon George,[ab] Sourava Chandra Pradhan,[ab] K. N. Narayanan Unni [ab] and Suraj Soman *[ab]

We have custom-engineered dye-sensitized solar cells (DSCs) by eliminating spacers and holes, fabricating hole-free, spacer-free (HF-SF) DSCs with a 96% active area to total area ratio. These newly engineered HF-SF dye cells provide better scalability, lower cost, and improved aesthetics with enhanced device performance delivering more than 30% efficiency under indoor/ambient illumination. Two serially interconnected HF-SF DSCs fabricated using D35:XY1b co-sensitized organic dyes and $[Cu^{(I/II)}(dmp)_2]$ electrolyte were able to autonomously power an indoor temperature and humidity monitoring unit free of batteries at realistic indoor illumination intensities below 200 lux.

Sustainability spotlight

Our innovative development of hole-free, spacer-free (HF-SF) dye-sensitized cells (DSCs) for indoor photovoltaic applications represents a significant sustainable advancement. Achieving efficiencies above 30%, our DSCs reduce the need for fluorine-doped tin oxide (FTO) glass substrates by 40% and electrolyte by 50%, cutting production costs and material use. This work aligns with UN Sustainable Development Goals 7 (affordable and clean energy) and 12 (responsible consumption and production) by offering a sustainable alternative to battery-powered devices. Our battery-free indoor weather monitoring unit mitigates 2440 g of CO_2 emissions by potentially reducing the need for 40 AAA batteries over a period of 10 years showcasing the potential of DSCs to reduce carbon emissions and environmental impact thereby promoting cleaner, more efficient energy solutions for a sustainable future.

DSCs have proved to be among the best photovoltaic technologies for indoor/ambient light harvesting applications, with efficiencies reaching above 35%.[1–9] Even though polymer based organic solar cells and perovskite solar cells have demonstrated promising photovoltaic (PV) results, they are still far behind the indoor PV capability of DSCs, especially from a sustainability point of view.[10–14] Since their inception in 1991, to date, these molecular light harvesters have been designed and fabricated using pre-drilled holes to facilitate electrolyte filling and polymeric films, epoxies and other insulating materials being used as spacers to separate the working and counter electrodes.[8,9,15–22] Precise drilling of holes requires laser-based machinery, making the module fabrication energy-consuming and less economical.[23–26] The long-term stability of these devices is also significantly determined by how best the holes are being sealed; hence, it critically limits the scale-up and commercialization aspects of DSCs. Besides, using spacers to separate the electrodes requires additional area, severely limiting the active area to total area ratio in conventional dye-sensitized solar modules (DSMs) to around 50%. This demands new architectural innovations to find alternate techniques that are more scalable and cost-competitive. Earlier, Boschloo and team proposed the benefits of reducing the inter-electrode spacing by fabricating devices where the photoanode and the counter electrode are placed in direct contact employing an insulating ZrO_2 layer.[27] Gratzel and co-workers also demonstrated using direct contact (DC) devices employing co-sensitized organic dyes and copper (Cu) redox mediators delivering higher PCEs under indoor illumination.[4] We have taken this one step further by not only removing the spacers but also eliminating the pre-drilled holes from the counter electrodes [Fig. 1(a and b)], thereby realizing DSCs with a 96% active area to total area ratio, better indoor photovoltaic performance, improved stability and superior aesthetics. The simplification of device fabrication, achieved by eliminating the hole-drilling process and spacers, has resulted in a refined procedure, enhancing its energy efficiency and economic viability.[28] This advancement opens up new avenues and opportunities for the potential commercialization of dye-sensitized light harvesters in indoor photovoltaics (IPV) and building integrated photovoltaics (BIPV) applications, thereby advancing their commercial viability.

[a]*Centre for Sustainable Energy Technologies (C-SET), CSIR-National Institute for Interdisciplinary Science and Technology, Thiruvananthapuram 695019, India*

[b]*Academy of Scientific and Innovative Research (AcSIR), Ghaziabad 201002, India. E-mail: suraj@niist.res.in*

† Electronic supplementary information (ESI) available. See DOI: https://doi.org/10.1039/d4su00434e

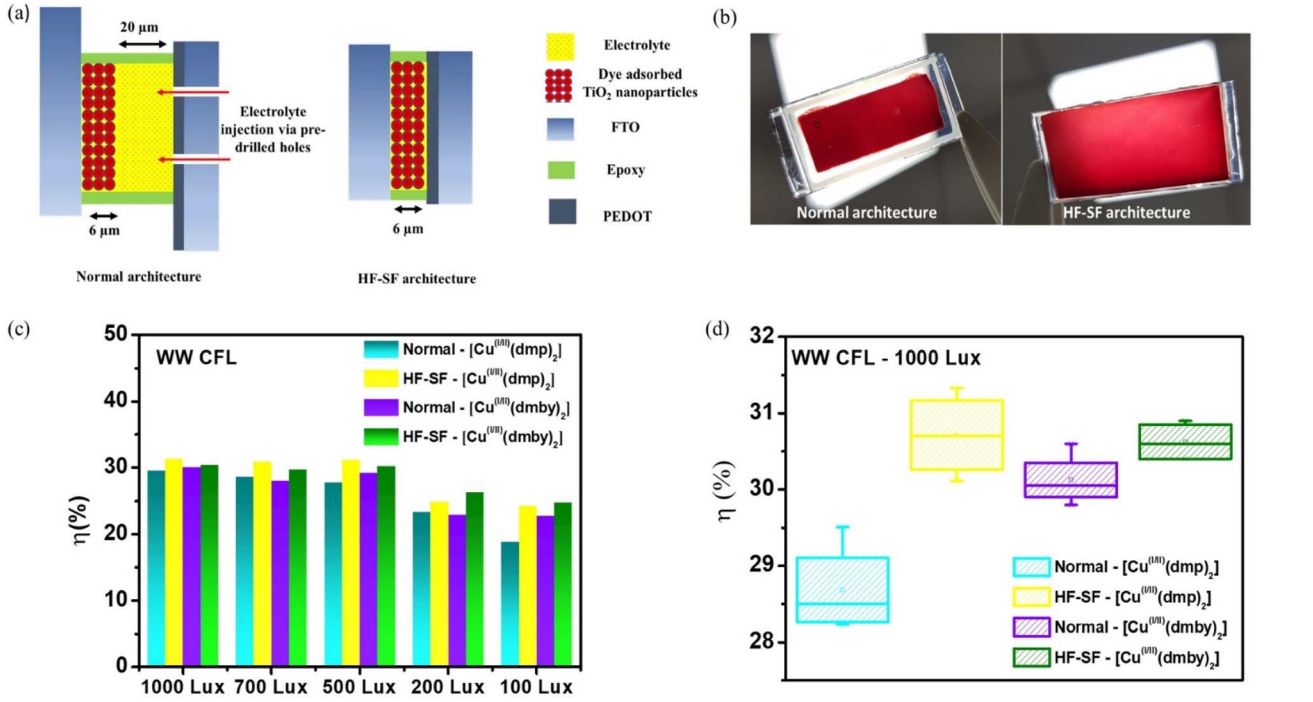

Fig. 1 (a) Schematic representation of normal and HF-SF DSC device architectures, (b) image of normal and HF-SF DSCs, (c) efficiency plot for D35:XY1b co-sensitized DSCs under WW CFL illumination (1000–100 lux) employing $[Cu^{(I/II)}(dmp)_2]$ and $[Cu^{(I/II)}(dmby)_2]$ electrolytes and (d) efficiency error plot for normal and HF-SF DSCs under WW CFL illumination (1000 lux) employing $[Cu^{(I/II)}(dmp)_2]$ and $[Cu^{(I/II)}(dmby)_2]$ electrolytes.

For initial optimizations, we used XY1b as the sensitizer and $[Cu^{(I/II)}(dmp)_2]$ as the redox electrolyte to compare the indoor photovoltaic performance between normal and HF-SF devices. The experimental section provides details on device fabrication and characterization. A schematic showing the various fabrication steps differentiating the two methods is also provided in the ESI† (Schemes S1a and b). Using the newly developed HF-SF device architecture and XY1b sensitizer, we were able to realize better short-circuit current density, J_{sc} (137.8 ± 4.99 μA cm^{-2}) and fill factor, FF (82.9 ± 1.5), contributing to an improved power conversion efficiency (PCE) of 30.48 ± 0.23% under standard 1000 lux warm white (WW) CFL illumination (Fig. S3 and Table S1, ESI†). Further, using D35:XY1b co-sensitized dyes, the PCE was improved to 31.33 ± 0.62% for the HF-SF DSCs compared to 29.51 ± 0.82% for the normal device (Fig. S4 and Table S2, ESI†). To further check the compatibility of the HF-SF device architecture with other alternative copper redox electrolytes, we replaced $[Cu^{(I/II)}(dmp)_2]$ with $[Cu^{(I/II)}(dmby)_2]$, and observed a similar trend with the HF-SF device outperforming the normal device with a PCE of 30.4 ± 0.22% under 1000 lux WW CFL illumination (Fig. S5 and Table S3, ESI†). A detailed investigation of photovoltaic parameters under various indoor illumination intensities (1000 lux, 700 lux, 500 lux, 200 lux, and 100 lux) using WW CFL and WW LED light sources is provided in Fig. 1(c) and S6, and Tables S4–S12, ESI†. Under all illumination intensities, using both Cu electrolytes, the HF-SF DSCs recorded better photovoltaic (PV) performance than the normal devices, with the variation more pronounced at lower intensities. The improvement in power conversion efficiency (PCE) for the HF-SF DSCs under CFL and LED lights using both copper electrolytes is mainly attributed to the improvement in short-circuit current density (Fig. S7 and S8, ESI†). Also, the PCE error plot (Fig. 1(d)) reveals better reproducibility for the HF-SF devices than normal devices. The deviation in device performance for the HF-SF devices arises from the variation in FF using $[Cu^{(I/II)}(dmp)_2]$ and variation in J_{sc} and FF employing $[Cu^{(I/II)}(dmby)_2]$ electrolyte (Fig. S9, ESI†). Improvement in FF was observed for the HF-SF DSCs fabricated using D35:XY1b co-sensitized dyes compared to the reported DC devices made using the Y123:XY1b combination, possibly due to the better dye coverage offered by the D35:XY1b co-sensitized dyes used in HF-SF DSCs.[4]

Extensive interfacial charge transfer measurements were carried out using electrical and optical perturbation tools (details provided in the experimental section) to probe the origin of variation in PV performance for the HF-SF devices. The shift in Fermi level was found to be negligible between the normal and HF-SF DSCs using both the copper electrolytes (Fig. 2(a)), and a similar trend was also observed for the transport time (Fig. 2(b)). This suggests that introducing the HF-SF architecture has little influence on the injection and electron transport within the mesoporous semiconductor. The lifetime measured using the Toolbox technique (Fig. 2(c)) showed improvement for the HF-SF DSCs using both $[Cu^{(I/II)}(dmp)_2]$ and $[Cu^{(I/II)}(dmby)_2]$ electrolytes which is a direct consequence of reducing the inter-electrode spacing, thereby reducing excess electrolyte in devices.[27] The impedance measurements carried out under dark conditions (Fig. 2(d)) reveal the first semicircle

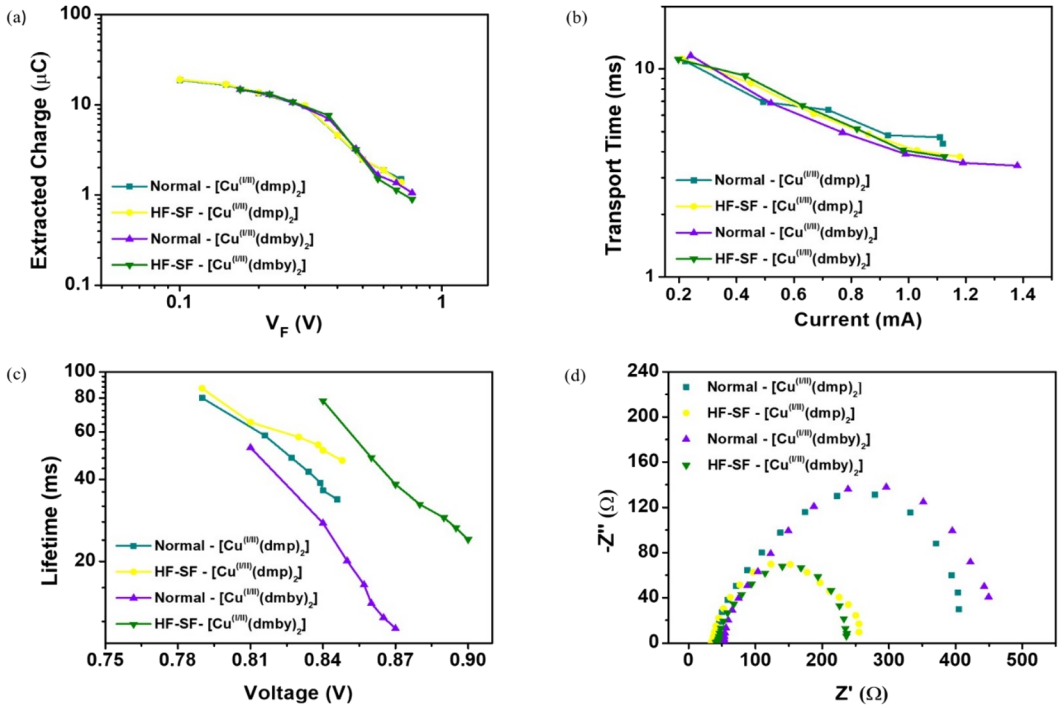

Fig. 2 (a) Charge extraction, (b) transport time (Toolbox), (c) lifetime (Toolbox), and (d) Nyquist plot (EIS) measurements for normal and HF-SF devices using $[Cu^{(I/II)}(dmp)_2]$ and $[Cu^{(I/II)}(dmby)_2]$ electrolytes.

in the high frequency region (charge transfer at the counter electrode/electrolyte interface) and the second semicircle in the middle frequency region (charge transfer at the TiO_2/dye/electrolyte interface) to be overlapping for the normal and HF-SF devices (for both copper redox systems), suggesting similar charge transfer kinetics for both device architectures. The only appreciable change visible is for the third semicircle, which corresponds to the ion diffusion in the electrolyte. For both copper redox systems, a larger third semicircle was observed for the normal device compared to the HF-SF DSCs, indicating higher diffusion resistance for the former.[29–31] The use of the new HF-SF device architecture provides an opportunity to address this bottleneck, improving the indoor PV performance of DSCs under ambient/indoor light conditions.

Further, we fabricated large-area DSCs having an active area of 1.92 cm^2 using the HF-SF architecture employing D35:XY1b co-sensitized dyes and $[Cu^{(I/II)}(dmp)_2]$ electrolyte. Large area DSCs fabricated using the HF-SF architecture delivered an impressive efficiency of 29.35 ± 0.09% compared to 25.34 ± 0.06% for the normal DSCs, as shown in Fig. 3(a). A detailed examination of the PV performance under various illumination intensities (1000 lux to 100 lux) was carried out for the large area DSCs under both WW CFL (Fig. 3(b) and Tables S13–S17, ESI†) and WW LED (Fig. S10, Tables S18–S22, ESI†) illuminations. Large area DSCs fabricated using the novel HF-SF architecture outperformed normal devices with an improved PV performance under all illumination conditions. The improvement in current density by 17.31% for HF-SF DSCs resulted in an enhancement in power output by 18.30% and an increase in efficiency by 18.25% under WW CFL illumination (Fig. S11, ESI†). A similar trend was observed under WW LED illumination with average increments of 14.39%, 13.93% and 14.98% for current density, power output and efficiency (Fig. S12, ESI†). The absolute error plots on the device parameters for large-area DSCs are provided in Fig. S13, ESI,† which indicate that the variation in current density for the normal devices was successfully addressed by switching over to the HF-SF devices using $[Cu^{(I/II)}(dmp)_2]$ electrolyte. Fig. 3(c) demonstrates a direct comparison of normal and HF-SF large-area DSCs for the same active area. The HF-SF device architecture facilitated a notable enhancement in the active area to total device area ratio, increasing it from 53% (in normal DSCs) to 96% in HF-SF DSCs. Consequently, this advancement resulted in a 40% reduction in the required quantity of FTO (fluorine-doped tin oxide) conductive glass substrates which accounts for ~80% of the total cost of these devices and a 50% decrease in electrolyte consumption, thereby contributing to a decreased production cost (Tables S23 and S24, ESI†). We have also found that large area HF-SF DSCs fabricated using conventional ruthenium dye (Z907) and commercial stable iodide/triiodide electrolyte (HSE) delivered a PCE of 15.95% under standard 1000 lux WW CFL illumination (Fig. S14 and Table S25, ESI†). This demonstrates the superior capability of co-sensitized organic dyes and copper electrolyte combination for indoor light harvesting applications. The stability of HF-SF DSCs was studied using accelerated testing done using a custom-made indoor stability testing unit (Fig. S15†) which maintained an average of 95% of its initial value under LED soaking for 1000 hours (Fig. S16, ESI†).

Dye-sensitized modules (DSMs) were fabricated by serially interconnecting two HF-SF devices. Under standard 1000 lux

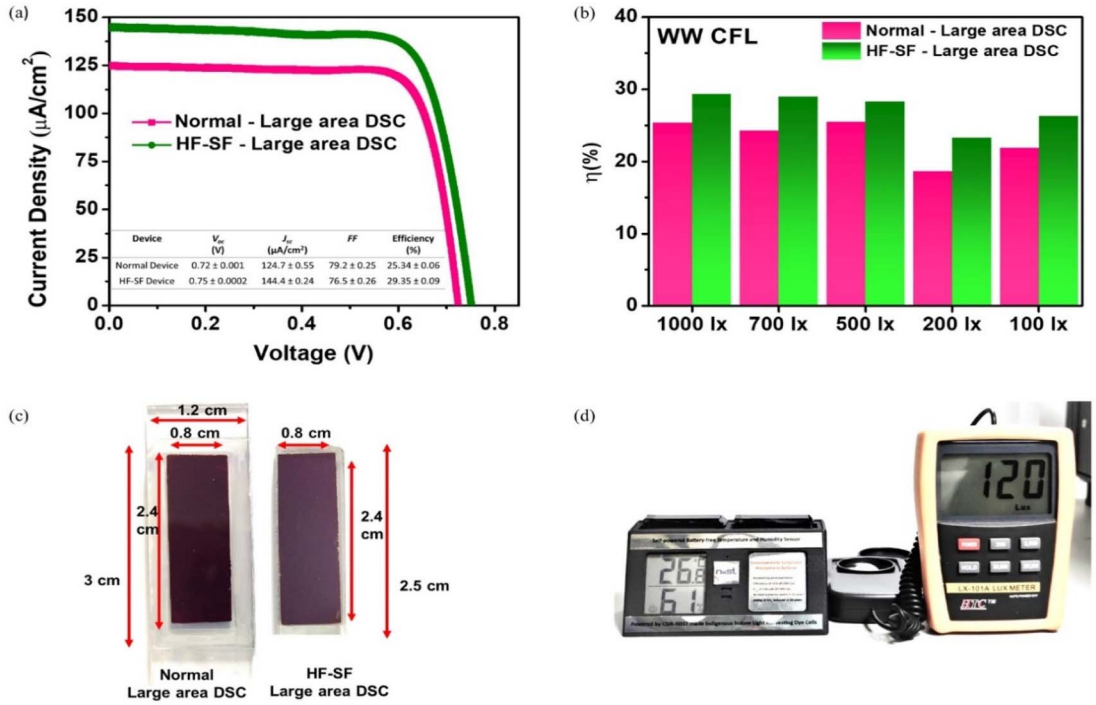

Fig. 3 (a) *J*–*V* graph for large area DSCs under 1000 lux WW CFL illumination (*J*–*V* data in the inset), (b) device performance of large area DSCs under WW CFL illumination (1000 lux–100 lux), (c) a comparison of normal large area DSCs with HF-SF large area DSCs and (d) a DSM made by serially interconnecting two large area DSCs powering an indoor weather monitoring unit (temperature and humidity sensor) under 120 lux indoor LED illumination.

WW CFL illumination, the serially connected HF-SF DSMs delivered a V_{oc} of 1.39 V, I_{sc} of 546.02 μA, and FF of 64% contributing to a remarkable power output of 485.9 μW (Table S26, ESI†) using D35:XY1b co-sensitized dyes and $[Cu^{(I/II)}(dmp)_2]$ electrolyte. The integration of DSMs was subsequently undertaken with a tailor-made power management circuit to create an autonomous indoor weather monitoring unit, specifically designed for temperature and humidity measurements, enabling us to completely replace two conventional AAA batteries, which are originally required to power the device (Scheme S2 and Fig. S17, ESI†). With a power output of 73 μW under a much lower indoor illumination of 120 lux (LED), we were able to autonomously power the sensor unit using our DSCs (Fig. 3(d), Video S1†). By eliminating holes and back sealing, HF-SF DSCs also open up new avenues to develop bifacial and multijunction DSCs. Using one layer of *meso*-TiO_2 (3 μm), under 1000 lux WW CFL illumination, HF-SF devices gave a remarkable PCE of 15.45% upon back side illumination against 2.51% using a normal device (Fig. S18 and Table S27, ESI†). Apart from better indoor device performance and lower fabrication cost, work is ongoing in our lab to utilize the bifacial and multijunction DSC stacks with improved aesthetics for building integrated photovoltaics.

The HF-SF DSCs with efficiencies above 30%, along with the reduction in the cost of production and ease of fabrication, have proven to be a preferable alternative to the existing normal devices, which can accelerate the commercialization of DSCs for indoor photovoltaics. To demonstrate the true potential of indoor HF-SF DSCs, we developed a self-powered indoor weather monitoring unit which can potentially mitigate 2440 g of CO_2 emission by eliminating the need for 40 AAA batteries over ten years, significantly reducing the environmental impact of discarded batteries and enabling a sustainable future through indoor/ambient light recycling.

Data availability

The data supporting this article have been included as part of the ESI† and are also available at [DOI:10.22541/AU.171184730.01468583].

Conflicts of interest

There are no conflicts to declare.

Acknowledgements

The authors acknowledge financial support from a DST-Solar Challenge Award (DST/ETC/CASE/RES/2023/05(C)/(G)) and CSIR-FTT project (FTT 060511).

Notes and references

1 D. Zhang, M. Stojanovic, Y. Ren, Y. Cao, F. T. Eickemeyer, E. Socie, N. Vlachopoulos, J. E. Moser, S. M. Zakeeruddin, A. Hagfeldt and M. Grätzel, *Nat. Commun.*, 2021, **121**(12), 1–10.

2 M. Freitag, J. Teuscher, Y. Saygili, X. Zhang, F. Giordano, P. Liska, J. Hua, S. M. Zakeeruddin, J. E. Moser, M. Grätzel and A. Hagfeldt, *Nat. Photonics*, 2017, **116**(11), 372–378.
3 R. Haridas, J. Velore, S. C. Pradhan, A. Vindhyasarumi, K. Yoosaf, S. Soman, K. N. N. Unni and A. Ajayaghosh, *Adv. Mater.*, 2021, **2**, 7773–7787.
4 Y. Cao, Y. Liu, S. M. Zakeeruddin, A. Hagfeldt and M. Grätzel, *Joule*, 2018, **2**, 1108–1117.
5 G. Gokul, S. C. Pradhan and S. Soman, *Energy, Environ. Sustain.*, 2019, 281–316.
6 H. Michaels, M. Rinderle, R. Freitag, I. Benesperi, T. Edvinsson, R. Socher, A. Gagliardi and M. Freitag, *Chem. Sci.*, 2020, **11**, 2895–2906.
7 Y. Ren, D. Zhang, J. Suo, Y. Cao, F. T. Eickemeyer, N. Vlachopoulos, S. M. Zakeeruddin, A. Hagfeldt and M. Grätzel, *Nature*, 2022, **613**, 60–65.
8 A. Jagadeesh, G. Veerappan, P. S. Devi, K. N. N. Unni and S. Soman, *J. Mater. Chem. A*, 2023, **11**, 14748–14759.
9 S. M. Meethal, S. C. Pradhan, J. Velore, S. Varughese, R. S. Pillai, F. Sauvage, A. Hagfeldt and S. Soman, *J. Mater. Chem. A*, 2024, **12**, 1081–1093.
10 X. He, J. Chen, X. Ren, L. Zhang, Y. Liu, J. Feng, J. Fang, K. Zhao and S. Liu, *Adv. Mater.*, 2021, **33**, 2100770.
11 W. Peng, K. Mao, F. Cai, H. Meng, Z. Zhu, T. Li, S. Yuan, Z. Xu, X. Feng, J. Xu, M. D. McGehee and J. Xu, *Science*, 2023, **379**, 683–690.
12 S. Zhang, F. Ye, X. Wang, R. Chen, H. Zhang, L. Zhan, X. Jiang, Y. Li, X. Ji, S. Liu, M. Yu, F. Yu, Y. Zhang, R. Wu, Z. Liu, Z. Ning, D. Neher, L. Han, Y. Lin, H. Tian, W. Chen, M. Stolterfoht, L. Zhang, W. H. Zhu and Y. Wu, *Science*, 2023, **380**, 404–409.
13 J. D. Azoulay, Z. A. Koretz, B. M. Wong and G. C. Bazan, *Macromolecules*, 2013, **46**, 1337–1342.
14 A. E. London, L. Huang, B. A. Zhang, M. B. Oviedo, J. Tropp, W. Yao, Z. Wu, B. M. Wong, T. N. Ng and J. D. Azoulay, *Polym. Chem.*, 2017, **8**, 2922–2930.
15 K. Kakiage, Y. Aoyama, T. Yano, K. Oya, J. I. Fujisawa and M. Hanaya, *Chem. Commun.*, 2015, **51**, 15894–15897.
16 S. Ito, T. N. Murakami, P. Comte, P. Liska, C. Grätzel, M. K. Nazeeruddin and M. Grätzel, *Thin Solid Films*, 2008, **516**, 4613–4619.
17 P. Wang, S. M. Zakeeruddin, J. E. Moser, M. K. Nazeeruddin, T. Sekiguchi and M. Grätzel, *Nat. Mater.*, 2003, **26**(2), 402–407.
18 A. Kay and M. Grätzel, *Sol. Energy Mater. Sol. Cells*, 1996, **44**, 99–117.
19 L. Wang, X. Fang and Z. Zhang, *Renew. Sustain. Energy Rev.*, 2010, **14**, 3178–3184.
20 Y. Takeda, N. Kato, K. Higuchi, A. Takeichi, T. Motohiro, S. Fukumoto, T. Sano and T. Toyoda, *Sol. Energy Mater. Sol. Cells*, 2009, **93**, 808–811.
21 A. Fakharuddin, R. Jose, T. M. Brown, F. Fabregat-Santiago and J. Bisquert, *Energy Environ. Sci.*, 2014, **7**, 3952–3981.
22 A. B. Muñoz-García, I. Benesperi, G. Boschloo, J. J. Concepcion, J. H. Delcamp, E. A. Gibson, G. J. Meyer, M. Pavone, H. Pettersson, A. Hagfeldt and M. Freitag, *Chem. Soc. Rev.*, 2021, **50**, 12450–12550.
23 L. Vesce, P. Mariani, M. Calamante, A. Dessì, A. Mordini, L. Zani and A. Di Carlo, *Sol. RRL*, 2022, **6**, 2200403.
24 C. Cornaro, S. Bartocci, D. Musella, C. Strati, A. Lanuti, S. Mastroianni, S. Penna, A. Guidobaldi, F. Giordano, E. Petrolati, T. M. Brown, A. Reale and A. Di Carlo, *Prog. Photovoltaics Res. Appl.*, 2015, **23**, 215–225.
25 S. Noda, K. Nagano, E. Inoue, T. Egi, T. Nakashima, N. Imawaka, M. Kanayama, S. Iwata, K. Toshima, K. Nakada and K. Yoshino, *Synth. Met.*, 2009, **159**, 2355–2357.
26 F. Ribeiro, J. MaçAira, R. Cruz, J. Gabriel, L. Andrade and A. Mendes, *Sol. Energy Mater. Sol. Cells*, 2012, **96**, 43–49.
27 R. García-Rodríguez, R. Jiang, E. J. Canto-Aguilar, G. Oskam and G. Boschloo, *Phys. Chem. Chem. Phys.*, 2017, **19**, 32132–32142.
28 S. Soman, A. S. George, S. Chandra Pradhan, K. N. Narayanan Unni and S. C. Pradhan, *Authorea*, 2024, DOI: **10.22541/au.171184730.01468583/v1**.
29 J. Velore, S. Chandra Pradhan, T. W. Hamann, A. Hagfeldt, K. N. N. Unni and S. Soman, *ACS Appl. Energy Mater.*, 2022, **5**, 2647–2654.
30 S. C. Pradhan, J. Velore, A. Hagfeldt and S. Soman, *J. Mater. Chem. C*, 2022, **10**, 3929–3936.
31 S. C. Pradhan, A. Hagfeldt and S. Soman, *J. Mater. Chem. A*, 2018, **6**, 22204–22214.